A methodology for the incorporation of arbitrarily-shaped feet in passive bipedal walking dynamics

Aikaterini Smyrli, *Student Member, IEEE*, and Evangelos Papadopoulos, *Fellow, IEEE*

Abstract— <mark>A methodology for implementing arbitrary foot shapes</mark> in the passive walking dynamics of biped robots is developed. The dynamic model of a walking robot is defined in a way that allows shape-dependent foot kinetics to contribute to the robot's dynamics, for all convex foot shapes regardless of the exact foot geometry: for the developed method, only the set of points describing the foot profile curve is needed. The method is mathematically derived and then showcased with an application. The open-source pose estimation system OpenPose is used to determine the foot profile that enables the rigid-foot passive robot to reproduce the ankle trajectory of the actively powered, multi-DOF human foot complex. The passive gait of the biped robot walking on the specified foot shape is simulated and analyzed, and a stable walking cycle is found and evaluated. The proposed model enables the study of the effects of foot shape on the walking dynamics of biped robots, eliminating the necessity of solely using simple, and analytically defined geometric shapes as the walking robots' feet. The method can be used for foot shape optimization towards achieving any desired walking pattern in walking robots.

I. INTRODUCTION

The dynamics of human locomotion are of great interest in the robotics community. As a species, our unique mode of locomotion presented us with an evolutionary advantage over competitors. In recent years, <mark>the development of dexterous</mark> walking robots has accelerated the advances in the area of designing locomotion machines. The biped configuration presents the added interest of understanding, mimicking, and potentially re-imagining our own walking modes.

The first passive walking machines were introduced by McGeer [1]. In his work, he showed that walking is a passive mode of the biped dynamics, and he investigated the effects of design decisions on the characteristics of gait.

The simplest walking machines studied included a hip mass, rigid legs with inertial elements and point feet [2][3]. McGeer's bipeds included hip joint friction and <mark>circular feet</mark> [1]. Alexander introduced axial leg compliance [4]. Other studies have included damping elements along the biped's compliant legs [5][6]. The trend of biomimetic design has inspired many researchers to study the effects of mimicking various other aspects of the human locomotion system in biped robots [7][8][9].

Along these lines, it has been proposed that the use of circular feet on rigid-legged walkers leads to human-like hip trajectories [10]. To date, the circle has been adopted for its simplicity as a foot shape in most of the works published on

The authors are with the School of Mechanical Engineering, National Technical University of Athens, (e-mail: egpapado@central.ntua.gr, tel: +30 210-772-1440).

bipedal locomotion. The effect of the circular foot shape on biped walkers' gait has been thoroughly investigated, and it has been shown that the passive bipeds' walking behavior changes with the circular foot's radius [1][6][11].

However, the human foot is not of circular shape. Instead, it consists of several joints in the ankle and in the ball of the foot, as well as in the foot's toes. As such, it is deformable and actively actuated during walking. Several humanoid robots have mimicked the multi-DOF actuated configuration of the human foot in their design [12][13][14].

In designing energetically efficient walking systems, as is the case for autonomous walking robots or gait-assisting devices and prostheses, it is important to minimize the energetic input required for locomotion. Towards this goal, passive foot designs have been proposed that mimic the human rollover geometry more closely than the originally proposed circular feet. A rigid flat foot has been studied as a means to simulate the double pivot around the heel and ball of the human foot during walking [15]. A foot shape consisting of two circular arcs at the heel and ball of the foot, connected by a linear part in the middle, has also been used for the simulation of the double pivot effect [16]. An elliptical foot shape has been proposed to model the gradual change in human rollover curvature [17].

The above closed-form foot shape geometries allow the simulation of walking for feet that are mathematically described by their respective geometries. A more generalized approach has been proposed for the modeling of passive gait on a more general foot shape [18]; however, the dynamics of the passive gait studied there include successive impacts at the points defining the foot shape curve, and subsequent pivots around each point until the next impact, as the next point hits the ground [18]. Such a model is inconsistent with the rolling motion of the human foot during walking.

In this paper, we propose a methodology for the simulation of passive gait dynamics for a biped robot model walking on feet of arbitrary shape. Any convex curve can be selected as a foot shape for the method. The gait produced can be evaluated with respect to any criterion and the points comprising the foot shape can be rearranged, optimizing the foot for the satisfaction of the selected criterion.

The dynamic modeling of the passive gait on the arbitrary feet is presented in Section II. In Section III, a foot shape is selected to obtain a human-like ankle trajectory, obtained with OpenPose. Section IV evaluates the passive gait produced by the biped for the selected foot shape. Finally, Section V presents the conclusion of the study.

II. GAIT MODELING

The dynamics of passive walkers are greatly influenced by their feet's interaction with the ground: the impact at heel strike (HS), the forward progression of the contact's center of

pressure, and finally the stance phase termination at the toe-off (TO) event, all depend on foot geometry and all contribute to the gait kinematics and dynamics.

For feet of certain geometric shapes, as is the circle or the ellipse, known geometric relations allow us to implement the foot-ground interaction within the dynamic equations governing gait. However, when foot geometry varies from explicitly defined shapes, the governing equations of the foot-ground interaction have to be expressed in a generalized way, to allow the calculation of the ground reaction forces and their implementation into the walking dynamics.

To generalize the gait dynamics description and solution, the biped is divided into two separate parts: the body and its dynamics model, and the foot and its kinetics model.

A. Body dynamics model

The *body dynamics* model is identical to all walkers regardless of foot shape and includes the two legs and their shared hip joint, but excludes the feet, see Fig. 1. The physical model includes all system inertial elements, i.e. the hip mass M as well as the leg masses m, situated at a distance l above the ankle positions A_1 and A_2 of each leg, and the axial-dynamics elements, i.e. the springs of elastic coefficient k and the dampers of damping coefficient b.
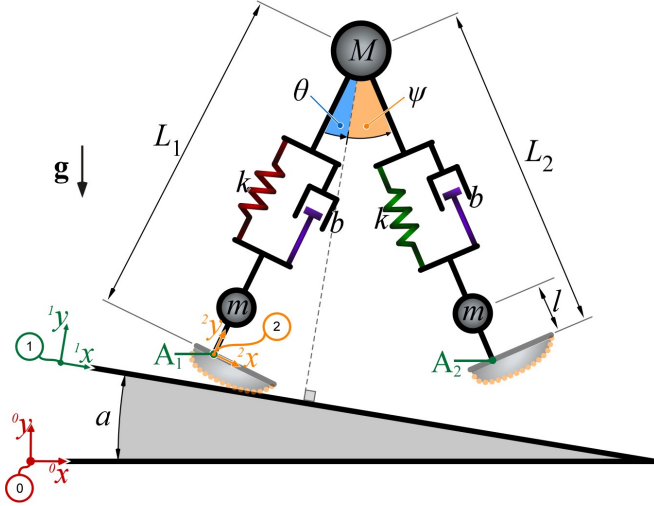

Figure 1. Body dynamics model.

Three coordinate systems (CS) are defined, see Fig. 1. The first, CS-0, is the inertial coordinate system, the second, CS-1, is sloped with respect to the first by an angle α, and the third, CS-2, is body-fixed on the stance leg at its ankle, point A_1. The body model of the biped has six degrees of freedom, namely the leg angles θ and ψ, the variable leg lengths L_1 and L_2 (both of uncompressed length L_{nat}), and the stance leg ankle A_1 position $(^1x_{A1}, {}^1y_{A1})$ defined in CS-1. These constitute the generalized coordinate vector $\mathbf{q}$:

$$\mathbf{q} = [{}^1x_{A1}, {}^1y_{A1}, \theta, L_1, \psi, L_2]^T \qquad (1)$$

The biped body operates under the gravitational pull g, acting on the inertial elements, and is subject to input forces acting on points A_1 and A_2, which constitute the interface with the foot part of the model.

As such, the motion of points A_1 and A_2, and by extension their spatial coordinates $(^1x_{A1}, {}^1y_{A1})$ and $(^1x_{A2}, {}^1y_{A2})$ respectively, are constrained during the times when their corresponding foot is in contact with the ground. This interaction is expressed in the form of algebraic constraint equations that must be satisfied by the biped's state.

The equations of motion are expressed in the form:

$$\mathbf{M(q)\ddot{q} + C(q,\dot{q})\dot{q} + K(q) + G(q) - f = 0} \qquad (2)$$
$$\mathbf{c(q) = 0}$$

where $\mathbf{M_{6x6}}$ is the mass matrix, $\mathbf{C_{6x6}}$ is a matrix containing centrifugal, Coriolis and damping terms, $\mathbf{K_{6x1}}$ is the elasticity vector, $\mathbf{G_{6x1}}$ is the gravity vector and $\mathbf{f_{6x1}}$ is the generalized constraint force vector. Finally, $\mathbf{c}$ is the vector containing the motion's algebraic constraints. Both $\mathbf{f}$ and $\mathbf{c}$ differ for the single ($\mathbf{f_{SSP}}$, $\mathbf{c_{SSP}}$) and double stance phase ($\mathbf{f_{DSP}}$, $\mathbf{c_{DSP}}$).

In the single stance phase (SSP), only the stance leg is in contact with the ground: Point A_1's coordinates are constrained as the stance foot rolls on the ground; then $\mathbf{f}$ takes the form:

$$\mathbf{f_{SSP} = \Pi_{SSP}(q)\lambda_{SSP}} \qquad (3)$$

where $\boldsymbol{\lambda}_{SSP}$ is a 2x1 Lagrange multiplier vector, with elements equal to the constraint reaction forces in each constraint's direction. $\mathbf{\Pi}_{SSP}$ is a 6x2 constraint Jacobian matrix that transforms the reaction forces $\boldsymbol{\lambda}_{SSP}$ defined in the direction of the constraints to generalized forces acting on the elements of $\mathbf{q}$. It is defined by:

$$\mathbf{\Pi}_{SSP} = \left(\frac{\partial \mathbf{c}_{SSP}}{\partial \mathbf{q}}\right)^T \qquad (4)$$

In (4), $\mathbf{c}_{SSP}$ is the SSP 2x1 algebraic constraint vector, which depends on $\mathbf{q}$ and on foot geometry, as will be seen in the next section.

On the other hand, both A_1 and A_2 are constrained during the double stance phase (DSP): both legs are in rolling contact with the ground and their coordinates are constrained. This leads to $\mathbf{c}_{DSP}$ being a 4x1 vector, resulting in $\mathbf{\Pi}_{DSP}$, a 6x4 constraint Jacobian that multiplies the 4x1 Lagrange multiplier vector $\boldsymbol{\lambda}_{DSP}$, finally resulting in the generalized constraint force vector $\mathbf{f}_{DSP}$. The above results from using the transcript 'DSP' instead of 'SSP' in (3) and (4).

Therefore, in order to solve the gait dynamics for feet of arbitrary geometry, constraint vectors $\mathbf{c}$ and Jacobians $\mathbf{\Pi}$ in both the SSP and DSP must be calculated.

B. Foot kinetics model

In the simplest case of circular feet of radius r, with an ankle A_r at $(^1x_{Ar}, {}^1y_{Ar})$ located at the center of the circle, the rolling contact constraints are simply:

$$c_{r1} = \Delta{}^1x_{Ar} - r\Delta\gamma = 0 \qquad (5)$$
$$c_{r2} = {}^1y_{Ar} - r = 0 \qquad (6)$$

where $\Delta{}^1x_{Ar}$ denotes the ^1x-displacement of the ankle between two instances, measured in CS-1; in a similar manner, $\Delta\gamma$ expresses the respective change in the leg's angle, γ.

Equations (5) and (6) analytically describe the kinematic relationship between the ankle DOFs of A_r and the foot angle γ. Since the constraint vector is $\mathbf{c_r} = [c_{r1}, c_{r2}]^T$, $\mathbf{\Pi}$ can be expressed analytically through (4), leading to an expression for $\mathbf{f}$ using (3). In this manner, all elements of (2) are expressed analytically in terms of state variables, and the dynamical system can be simulated.

Similar geometric expressions for foot kinetics can lead to analytical descriptions of gait dynamics for various other foot geometries [17]. However, when aiming to optimize foot geometry for a certain criterion, the optimal foot shape might

not be of a specifically defined geometry: instead, we might only be able to express such an optimal foot shape in a numerical manner, as for example a set of points in the plane.

Let P be a set of points in the form $P_i(^2x_i, ^2y_i)$, describing the arbitrary foot shape's profile coordinates, expressed in the foot-bound coordinate system (^2x, ^2y) with its origin at the foot's ankle, A^*, as shown in Fig. 2.

For foot shapes with convex geometry profiles, the foot is always tangent to the floor at the point of contact. Therefore, for a foot rotated by γ, we can look for point C of the foot that will be in contact with the ground, where:

$$\tan(\gamma) = \left.\frac{d(^2y)}{d(^2x)}\right|_C \quad (7)$$

Figure 2. Foot kinetics model.

Since the foot's profile is a convex curve, only one point of the foot profile satisfies (7): we identify this as the point of contact, $^2C(^2x_C, ^2y_C)$. It follows that for a given foot geometry, the coordinates of C only depend on γ. The contact point C defines the foot profile angle at C, $^2\varphi_C$:

$$\tan(^2\varphi_C) = \frac{^2y_C}{^2x_C} \quad (8)$$

Moreover, the contact point's distance from point A, ^2r_C, is:

$$^2r_C = \sqrt{\left(^2x_C\right)^2 + \left(^2y_C\right)^2} \quad (9)$$

Let γ_{HS} be the foot angle at the start of the ground contact at HS, and let the HS contact point be positioned at $^1x_{HS}$ in the CS-1. At a later instance, the foot angle has increased to γ and the contact point in CS-1 has moved to ^1x_C:

$$^1x_C = {}^1x_{HS} + \int_{\gamma_{HS}}^{\gamma} \sqrt{\left(\frac{d(^1x)}{d(\gamma)}\right)^2 + \left(\frac{d(^1y)}{d(\gamma)}\right)^2}\, d(\gamma) \quad (10)$$

If C_{HS} is the foot point in contact with the floor at HS, and C is the contact point for a foot angle γ, Eq. (10) displaces the floor contact point by a distance equal to the length of the foot profile curve between C_{HS} and C; this is assuming that there is no slippage at the foot-floor contact.

Based on the above, the arbitrary foot's ankle position in CS-1, as it is obtained through the rolling contact for a inclination γ (superscript *), is only a function of γ, and it can be written as $^1A^*(^1x_A^*, ^1y_A^*)$, where:

$$^1x_A^* = {}^1x_C - {}^2r_C \cos(\gamma - {}^2\varphi_C) = {}^1x_A^*(\gamma) \quad (11)$$

$$^1y_A^* = {}^2r_C \sin(\gamma - {}^2\varphi_C) = {}^1y_A^*(\gamma) \quad (12)$$

Our goal is to find the constraint vector $\mathbf{c}_A$ imposed on the arbitrary foot's ankle coordinates in CS-1, ^1x_A and ^1y_A. These coincide with the ankle positions due to the rolling contact, $^1x_A^*$ and $^1y_A^*$ respectively:

$$\mathbf{c}_A = \begin{bmatrix} c_1 \\ c_2 \end{bmatrix} = \begin{bmatrix} ^1x_A \\ ^1y_A \end{bmatrix} - \begin{bmatrix} ^1x_A^*(\gamma) \\ ^1y_A^*(\gamma) \end{bmatrix} = \mathbf{0} \quad (13)$$

It can be seen that $\mathbf{c}_A$ consists of two distinct parts: a part that is a function of the ankle's DOFs, and a second part that is a function of the foot angle γ.

C. Stance foot constraints

The biped's stance foot is in contact with the ground in both SSP and DSP. The constraint scenario studied above is exactly analogous to the constraints acting on the stance foot, where $\gamma = \theta$: therefore $\mathbf{c}_{SSP} \equiv \mathbf{c}_A = [c_1, c_2]^T$. Knowing $\mathbf{c}_{SSP}$, $\mathbf{\Pi}_{SSP}$ can be calculated through (4):

$$\mathbf{\Pi}_{SSP} = \begin{bmatrix} 1 & 0 & -\partial\left(^1x_{A1}^*\right)/\partial\theta & 0 & 0 & 0 \\ 0 & 1 & -\partial\left(^1y_{A1}^*\right)/\partial\theta & 0 & 0 & 0 \end{bmatrix}^T \quad (14)$$

We have defined $\mathbf{\Pi}$ as $\mathbf{\Pi}(\mathbf{q})$, therefore all terms in (14) should be expressed as a function of the elements of $\mathbf{q}$. However, (11) and (12) that are to be differentiated for (14) include the contact angle $^2\varphi_C$, defined in (8). The relation of $^2\varphi_C$ to $\theta = \gamma$ is not mathematically straightforward: to calculate the term $\partial(^2\varphi_C)/\partial\theta$, we set:

$$\kappa = \tan\left(^2\varphi_C\right) = \frac{^2y_C}{^2x_C} \Rightarrow {}^2\varphi_C = \tan^{-1}\kappa \quad (15)$$

and using the chain rule, we find:

$$\frac{\partial}{\partial\theta}{}^2\varphi_C \overset{(15)}{=} \frac{1}{1+\kappa^2}\frac{\partial\kappa}{\partial\theta} = \frac{1}{1 + \left(\frac{^2y_C}{^2x_C}\right)^2}\frac{\partial\kappa}{\partial\theta} \quad (16)$$

Differentiating κ in (15) and updating (16) results in (17):

$$\frac{\partial}{\partial\theta}{}^2\varphi_C = \left(\frac{^2x_C\frac{\partial}{\partial\theta}{}^2y_C - {}^2y_C\frac{\partial}{\partial\theta}{}^2x_C}{\left(^2x_C\right)^2 + \left(^2y_C\right)^2}\right) \quad (17)$$

Similarly, for the derivative of ^2r_C with respect to θ:

$$\frac{\partial}{\partial\theta}{}^2r_C \overset{(9)}{=} \left(\frac{^2x_C\frac{\partial}{\partial\theta}{}^2x_C + {}^2y_C\frac{\partial}{\partial\theta}{}^2y_C}{\sqrt{\left(^2x_C\right)^2 + \left(^2y_C\right)^2}}\right) \quad (18)$$

The terms ^2x_C, ^2y_C in (17) and (18) depend only on θ through (7). Their partial derivatives with respect to θ can be numerically estimated for every meaningful θ, that is $\theta \in [-90°, +90°]$. Therefore, all terms of (13) can be differentiated with respect to, and $\mathbf{\Pi}_{SSP}$ in (14) can be expressed numerically for every θ.

D. Numerical considerations for finite foot shapes

Some foot geometries may not cover the full range of θ's 180° span as defined here: for example, the derivative of a finite curve's endpoint is not defined, see point B in Fig. 2. At the same time, no point in the foot curve is tangent to the ground for a foot inclination θ_B, as shown in Fig. 3. It is intuitive, however, that for a foot angle θ_B, it is point B that will be in contact with the ground, and the foot will be pivoting around it until θ obtains a value such that point C can be defined through (7).
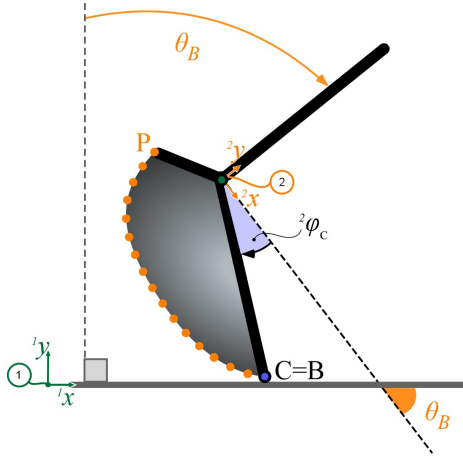
Figure 3. Foot kinetics for large inclination.

E. Swing foot constraints

The swing leg meets the ground at HS and is thereafter constrained to roll on the ground until TO. The swing foot constraints are added to the stance foot constraints to form the DSP constraint vector $\mathbf{c}_{DSP}=[c_1, c_2, c_3, c_4]^T$, where c_3 and c_4 can be found similarly to the process presented in the previous section, for $\gamma = -\psi$:

$$\begin{bmatrix} c_3 \\ c_4 \end{bmatrix} = \begin{bmatrix} {}^1x_{A1} + L_1 \sin\theta + L_2 \sin\psi \\ {}^1y_{A1} + L_1 \cos\theta - L_2 \cos\psi \end{bmatrix} - \begin{bmatrix} {}^1x_{A2}^* (-\psi) \\ {}^1y_{A2}^* (-\psi) \end{bmatrix} \quad (19)$$

where the minus sign of ψ is due to the opposite definition of angles θ and ψ. Similarly to (13), the first set of terms in (19) is due to the biped's DOF configuration, while the second is due to the rolling contact.

The above result in $\mathbf{\Pi}_{DSP}$ through (4). The elements of $\mathbf{\Pi}_{DSP}$ are spared here due to space limitations.

F. Gait phase transitions

A walking step is defined to start with the beginning of the SSP; the corresponding initial conditions are an input to the solution. Let the state vector $\mathbf{x}_n$ at the beginning of the nth step be:

$$\mathbf{x}_n = [\mathbf{q}^T, \dot{\mathbf{q}}^T]^T_n \quad (20)$$

The gait dynamics are solved with the SSP constraints on the stance leg, until the HS event, which is defined as the moment the swing foot touches the ground, i.e. $c_4 = 0$, see (19). To avoid the "scuffing" of the swing foot on the ground during its forward motion due to the lack of knees, we also impose the swing foot advancement condition, $\psi > 0$, and the swing foot retraction position, $\dot{\psi} < 0$ in order for HS to occur. By definition, $\mathbf{c}_{DSP} = 0$ at HS. Similarly to (20), the state vector at HS of the nth step is $\mathbf{x}_{n,HS}$. We name f_{DSP} the mapping of $\mathbf{x}_n$ to $\mathbf{x}_{n,HS}$ through the SSP dynamics:

$$\mathbf{x}_{n,HS} = f_{SSP}(\mathbf{x}_n) \quad (21)$$

After HS, the DSP constraints are imposed on the biped, until the TO event. The initial conditions of the DSP are $\mathbf{x}_{n,HS}$. During DSP, the ground support is gradually transferred from the stance leg to the swing leg, until all of the biped's weight is supported by the swing leg. Therefore, the TO event occurs when the normal force of the stance leg's contact with the ground becomes zero. At TO, $\mathbf{c}_{SSP}=0$ both legs are in contact with the ground. If $\mathbf{x}_{n,TO}$ is the biped state at TO, we call f_{DSP} the DSP mapping:

$$\mathbf{x}_{n,TO} = f_{DSP}(\mathbf{x}_{n,HS}) \quad (22)$$

After TO, the $(n+1)^{th}$ step begins at the next SSP and the state is transformed to account for the left-right leg switch: the $(n+1)^{th}$ step's swing leg is the nth step's stance leg and vice versa. After the switch, the state is $\mathbf{x}_{n+1}$. We call a *gait function*, $\mathbf{G}$, the mapping of $\mathbf{x}_n$ to $\mathbf{x}_{n+1}$:

$$\mathbf{x}_{n+1} = \mathbf{G}(\mathbf{x}_n) \quad (23)$$

G. Solving the gait dynamics

Both in the SSP and in the DSP, the gait dynamics are of the form (2). This system of equations is a differential algebraic equation (DAE) system of index 2, as the constraints would need to be twice differentiated in order to turn the algebraic equations into ordinary differential equations (ODE) [22].

To solve the index 2 system, we differentiate $\mathbf{c}$ in (2) once with respect to time. Hence, we obtain:

$$\mathbf{M}(\mathbf{q})\ddot{\mathbf{q}} + \mathbf{C}(\mathbf{q},\dot{\mathbf{q}})\dot{\mathbf{q}} + \mathbf{K}(\mathbf{q}) + \mathbf{G}(\mathbf{q}) - \mathbf{f} = 0$$
$$\dot{\mathbf{c}}(\mathbf{q}) = 0 \quad (24)$$

At the first instance of the SSP, which is coincident with the previous step's TO event, the SSP constraints are satisfied, and $\mathbf{c}_{SSP} = 0$. Since in (24) the rate of change $\dot{\mathbf{c}}$ is zero, $\mathbf{c}_{SSP}$ will remain zero throughout SSP, and therefore the system in (24) is equivalent to the one in (2). The same holds for DSP. This leaves us with an index 1 DAE system.

It is significant to note that further differentiation of the constraints in (24) would result in an ODE system that would be simpler to solve. However, that system would not be the same as (2), as the original constraints would be violated: by setting $\ddot{\mathbf{c}} = 0$, we would be keeping $\dot{\mathbf{c}}$ constant, but $\dot{\mathbf{c}}$ is not necessarily zero at the HS and TO events, therefore $\mathbf{c}$ would change from its initial zero value as time progressed.

Finally, using the chain rule, we find:

$$\dot{\mathbf{c}}(\mathbf{q}) = \frac{\partial \mathbf{c}}{\partial \mathbf{q}} \dot{\mathbf{q}} \overset{(4)}{=} \mathbf{\Pi}^T \dot{\mathbf{q}} \quad (25)$$

The DAE system (24) then can be written:

$$\begin{bmatrix} \mathbf{I}_{6x6} & \mathbf{0}_{6x6} & \mathbf{0}_{6xN} \\ \mathbf{0}_{6x6} & \mathbf{M}_{6x6} & -\mathbf{\Pi}_{6xN} \\ \mathbf{\Pi}^T_{Nx6} & \mathbf{0}_{Nx6} & \mathbf{0}_{NxN} \end{bmatrix}_z \begin{bmatrix} \dot{\mathbf{q}}_{6x1} \\ \ddot{\mathbf{q}}_{6x1} \\ \lambda_{Nx1} \end{bmatrix}_{z+1} = \begin{bmatrix} \dot{\mathbf{q}}_{6x1} \\ -\mathbf{B}_{6x1} \\ \mathbf{0}_{Nx1} \end{bmatrix}_z \quad (26)$$

where $N=2$ for the SSP and $N=4$ for the DSP, z denotes the zth time step of the numerical integration, and $\mathbf{B}$ is given by:

$$\mathbf{B}(\mathbf{q},\dot{\mathbf{q}}) = \mathbf{C}(\mathbf{q},\dot{\mathbf{q}})\dot{\mathbf{q}} + \mathbf{K}(\mathbf{q}) + \mathbf{G}(\mathbf{q}) \quad (27)$$

The final form of the system (26) is solvable by DAE solvers, such as those in MATLAB. Here we have used ode23t for the SSP, and ode15s for the DSP, as the latter is more suitable for the stiff impact response of the DSP.

III. SELECTING THE FOOT SHAPE GEOMETRY

The generalized model presented in the previous section has been validated through comparison tests using the already developed models for circular and elliptical foot shapes, for which there exist analytically expressed dynamic models [6][17]. However, this model is of use when the foot under study is of a different shape, or even not analytically describable by a known geometric shape. This is the case for the human rollover shape.

A. Foot shape specifications

Rollover shapes were proposed as a means to simulate the effect of ankle joints on the kinetics and dynamics of bipedal walkers [19]. In most cases, circles have been used for their simplicity. However, as seen in (6), a circle's center stays at the same height during rollover, whereas the human ankle's trajectory is more complex. Elliptic foot shapes lead to 2-dimensional ankle trajectories, but only allow for 2 shaping parameters, leading to constrains in ankle trajectory. Our goal here is to find a rigid foot geometry to be used for the biped, that will lead to a human-like ankle trajectory.

The absence of compliance in the biped's feet means that a biped foot identical to the human foot in its flex state would lead to an unnatural ankle trajectory. To find the foot shape that fits the purpose, first we must obtain a measurement of a human foot's ankle trajectory during gait.

B. Ankle trajectory estimation with OpenPose

OpenPose [20][21] is an open-source pose estimation system that detects a set of keypoints on any given image of a human body. Here we have used OpenPose on a video recording of a step to obtain an estimation of the human ankle's trajectory on the sagittal plane during the stance foot's contact with the ground, see Fig. 4.
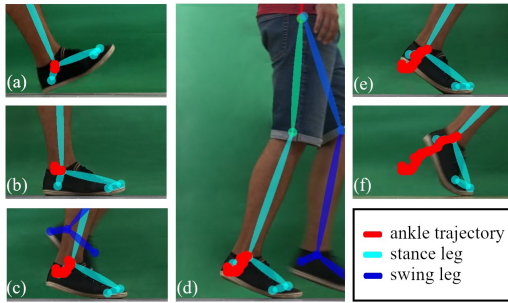

Figure 4. (a-f) Selected frames from OpenPose output for step video sequence. Stance leg in cyan, swing leg in blue. Ankle trajectory in red.

The ankle trajectory can be roughly approximated by an initial descent from HS until the foot is flat on the ground, which smoothly transitions to a circular arc of large radius, that lifts the ankle from the ground to prepare the foot for TO. The circular lift off corresponds to a pivoting motion around the ball of the foot. The human ankle is closer to the heel than to the ball pivot, hence the larger radius of the second part of the trajectory.

The ankle trajectory estimation using OpenPose is subject to detection errors, leading to a noisy trajectory, as can be seen in Fig. 4. However, here we are interested in approximating the trajectory's main trends with a smooth curve, which is not influenced by the exact ankle position at each frame.

C. Foot shape design

The next goal is to identify the rigid foot shape that results in the specified ankle trajectory when in rolling contact with the ground. For this reason, an interactive GUI was developed using MATLAB, allowing the speedy calculation of the ankle's trajectory for a foot shape defined by a set of points that can be interactively placed on CS-2. Eqs. (7) to (12) were used for this calculation.

The user closes the design loop by empirically placing the interactive points in a position that leads to the desired ankle trajectory. Finally, these selected points can be used to obtain an interpolated set of points that constitute a convex curve, to be used as the biped's foot shape. Fig. 5 (a) shows the final foot shape and (b) its ankle's trajectory, as the foot rolls on the ground, which approximates the measured data. Fig. 5 (b) distinguishes between a partial and a full foot rotation, as only part of the foot's total $180°$ rotation leads to the specified ankle trajectory.
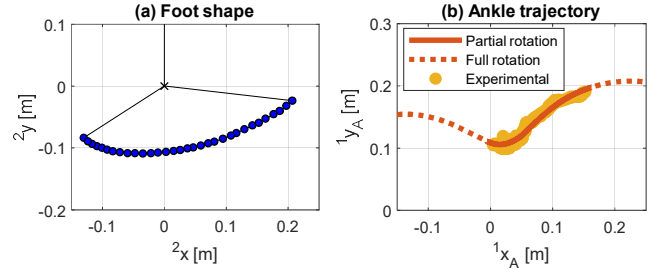

Figure 5. (a) Points defining the foot shape. (b) Biped ankle trajectory for full and partial rotation, compared to experimental data from OpenPose.

When rolling on the ground in a clockwise direction, the foot shape of Fig. 5 (a) initially pivots around its heel, as there is no contact point $(^2x_C, ^2y_C)$ on the foot profile that satisfies (7) for large negative γ values. During this time, the ankle forms a circular trajectory around the heel pivot, until Eq. (7) is first satisfied for an inclination angle $\gamma = -33°$. At this point, the foot starts rolling on its curved profile, until the foot's toe comes in contact with the ground at $\gamma = 38°$. The foot then pivots around the toe point for the remaining range of γ angles, again forming a circular trajectory. Since the foot shape is not symmetrical around the ankle, the two circular trajectories are of different radii, with the toe pivot having a larger radius than the heel pivot.

IV. WALKING ON ARBITRARY FOOT SHAPES

Up to this point, the methodology of combining foot kinetics with the biped dynamics to simulate walking on feet of arbitrary shape has been fully described, and a foot geometry has been decided for our simulations. In this section, the passive gait of the biped on the selected foot geometry is studied for its ability to perform stable passive gait as well as for the validity of the no-slip assumption made during the foot kinetics model's development. To realize the above, the derived foot shape must be incorporated in the biped model.

A. Incorporating the selected foot shape

The foot shape that was determined in Section III is made up of interpolated points P, as these were defined in Section II. Following the methodology described in Section II, we construct a lookup table to match all values of foot angle θ in the range $[-90°, +90°]$ to the contact point C through Eq. (7). A similar lookup table can be constructed for the swing leg angle ψ. Consequently, we can use these values to numerically calculate the foot shape geometric derivatives that are present in (14) and obtain for every configuration $\mathbf{q}$ a numerical expression of $\mathbf{\Pi}$, to be used in the DAE system (26). In this way, the foot kinetics are incorporated numerically in the biped dynamics.

B. *Investigation of walking capabilities*

The biped studied here has been studied analytically in [6] for the simple case of circular feet and in [17] for the case of elliptical feet. The model parameters used for the biped having the foot shape proposed in Section III are listed in Table I, with reference to Fig. 1.

It has been observed that the foot shape of biped robots affects their ability to perform stable walking [17]. Therefore, it is important to study the identified foot shape, and to investigate its potential to perform a stable passive walk.

TABLE I.   BIPED PARAMETERS.

Parameter	Explanation	Nominal Value
M	Biped body mass	80 [kg]
L_{nat}	Natural leg length	0.98 [m]
a	Floor slope	-3 [°]
b	Damping constant	800 [Ns/m]
k	Elastic constant	25,000 [N/m]
l	Foot mass distance from ankle	0.00 [m]
m	Foot mass	2.8 [kg]

The search for the biped's stable walking function includes determining the stable fixed points of **G** in (23); this process has been thoroughly presented in [6] and [17], and is not be repeated here. A stable gait cycle was identified for the biped of Table I with the foot shape of Fig. 5. The biped's convergence towards a stable gait is demonstrated in Fig. 6 (a), where one leg's angular DOF phase space is plotted for 100 consecutive steps of the biped. As can be seen in Fig. 6 (a), even though the initial conditions of the first step are outside the identified fixed-point trajectory, the biped's dynamics quickly converge towards that trajectory. The same holds for other initial conditions that lie near different areas of the limit cycle, as can be observed in Figs. 6 (b-d): the biped's gait always converges to the same stable trajectory.
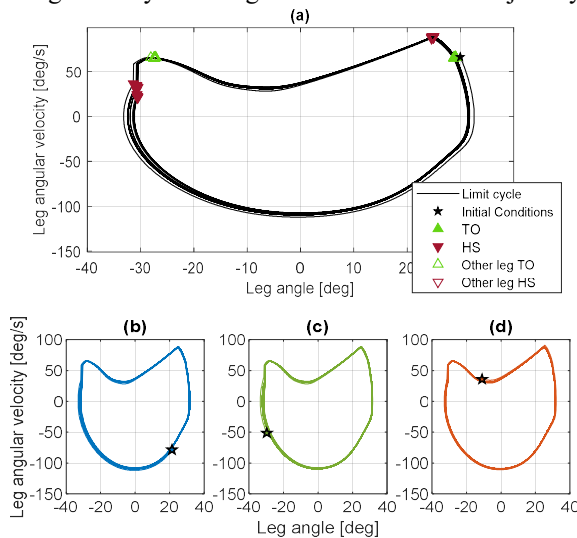

Figure 6. (a) Convergence to stable gait for a biped of the specified foot geometry, over 100 consecutive steps. (b-d) Various initial conditions outside the fixed-point trajectory are tested.

C. *Foot-ground interface forces*

It has been shown that the foot shape of biped robots influences the forces developed in the contact of the feet with the ground [17]. Furthermore, one of the assumptions used in the walking model developed was that there is no slippage of the biped's foot in its contact with the ground. This assumption is only valid if the contact's friction to normal force ratio is smaller than the static friction coefficient of the feet with the ground. As a result, the study of the ground reaction forces with respect to the foot and ground materials is important in a biped having an arbitrary foot profile.

As previously mentioned, the reaction force vector of a set of constraints **c** is the Lagrange multiplier vector **λ**. Fig. 7 shows the ground reaction forces for five consecutive steps of the biped, for a foot starting at SSP. The HS and TO events for the foot have been marked in the figure.
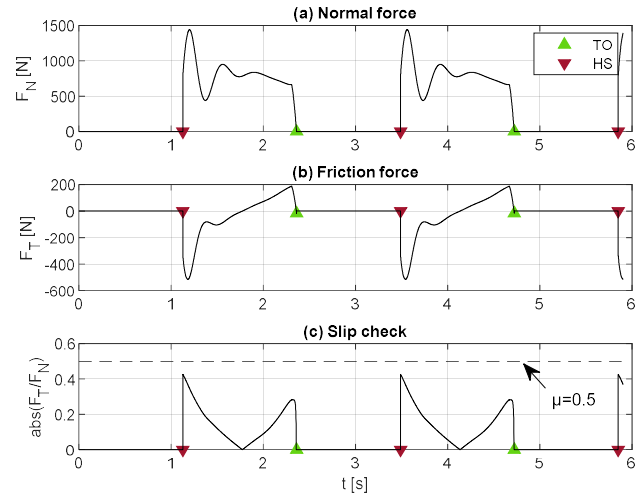

Figure 7. (a-b) Ground reaction forces and (c) friction coefficient for a foot during walking. As $F_T/F_N < \mu=0.5$, the biped does not slip.

It can be observed that both the normal force F_N and the peak friction force F_T following the foot's HS event, are both zero during the time the leg is in swing phase, i.e. between the TO and HS events. Their absolute ratio, which must be smaller than the coefficient of static friction μ, obtains a maximum value of about 0.4. Therefore, for $\mu=0.5$ the foot will not slip on the ground: this is achievable for many material combinations. Therefore, the model's no-slip assumption is valid for the selected foot shape.

V. CONCLUSION

In this paper, a methodology was developed that allows the incorporation of arbitrary foot shapes in the gait dynamics model of a passive bipedal walking robot.

The mathematical model for the gait was derived under a no-slip assumption for any convex foot geometry given as a set of 2D points. The model was tested on a custom foot shape, optimized so that the biped's ankles follow the trajectory of a human subject's recorded ankle motion.

Using the walking model, we were able to check the arbitrary-foot biped for its ability to perform stable passive gait, as well as for the validity of the no-slip assumption. Both these checks should follow any implementation of a random foot geometry in biped robots, to assure that the model is valid as well as that a real-world biped will be able to perform passive walking in an experimental environment.

The proposed methodology can be an iteration of a design loop to enable custom foot shape optimization, to better equip biped robots for different tasks, and to increase prosthetic devices' design suitability for personalized walking modes.

References

[1] McGeer, T., "Passive Dynamic Walking," *The International Journal of Robotics Research*, 1990. 9(2): pp. 62-82.

[2] Garcia, M., et al., "The Simplest Walking Model: Stability, Complexity, and Scaling," *Journal of Biomechanical Engineering*, 1998, 120(2): pp. 281-288.

[3] Espiau, B., and Goswami, A., "Compass gait revisited," *IFAC Proceedings Volumes*, 1994, 27(14): pp. 839-846.

[4] Alexander, R., "A model of bipedal locomotion on compliant legs," *Philosophical Transactions of the Royal Society of London, Series B: Biological Sciences*, 1992, 338(1284): pp. 189-198.

[5] Linde, R.Q.V.D., "Active leg compliance for passive walking," *IEEE International Conference on Robotics and Automation (ICRA '98)*, Leuven, Belgium, 1998, pp. 2339-2344.

[6] Smyrli, A., Bertos, G. and Papadopoulos, E., "Efficient stabilization of zero-slope walking for bipedal robots following their passive fixed point trajectories," *IEEE International Conference on Robotics and Automation (ICRA '18)*, Brisbane, Australia, 2018, pp. 5733-5738.

[7] McGeer, T., "Passive walking with knees," *IEEE International Conference on Robotics and Automation (ICRA '90)*, Cincinati, OH, USA, 1990, pp. 1640-1645.

[8] Asano, F., and Luo, Z. W., "Underactuated virtual passive dynamic walking with an upper body," *IEEE International Conference on Robotics and Automation (ICRA '08)*, Pasadena, CA, USA, 2008, pp. 2441-2446.

[9] Hanazawa, Y., et al., "High-speed limit cycle walking for biped robots using active up-and-down motion control of wobbling mass," *IEEE/RSJ International Conference on Intelligent Robots and Systems (IROS '13)*, Tokyo, Japan, 2013, pp. 3649-3654.

[10] Gard, S.A. and Childress, D.S., "What Determines the Vertical Displacement of the Body During Normal Walking?," *Journal of Prosthetics and Orthotics*, 2001, 13(3): pp. 64-67.

[11] Asano, F. and Luo, Z.W., "The effect of semicircular feet on energy dissipation by heel-strike in dynamic biped locomotion," *IEEE International Conference on Robotics and Automation (ICRA '07)*, Rome, Italy, 2007, pp. 3976-3981.

[12] Ouezdou, F. B., Alfayad, S., and Almasri, B., "Comparison of several kinds of feet for humanoid robot," *IEEE-RAS International Conference on Humanoid Robots (Humanoids '05)*, Tsukuba, Japan, 2005, pp. 123-128.

[13] Davis, S. and Caldwell, D. G., "The design of an anthropomorphic dexterous humanoid foot," *IEEE/RSJ International Conference on Intelligent Robots and Systems (IROS '10)*, Taipei, Taiwan, 2010, pp. 2200-2205.

[14] Narioka, K., Homma, T., and Hosoda, K., "Humanlike ankle-foot complex for a biped robot" *IEEE-RAS International Conference on Humanoid Robots (Humanoids '12)*, Osaka, Japan, 2012, pp. 15-20.

[15] Kwan, M., and Hubbard, M., "Optimal foot shape for a passive dynamic biped," *Journal of Theoretical Biology*, 2007, 248(2): pp. 331-339.

[16] Yamane, K., and Trutoiu, L., "Effect of foot shape on locomotion of active biped robots," *IEEE-RAS International Conference on Humanoid Robots (Humanoids '09)*, Paris, France, 2009, pp. 230-236.

[17] Smyrli, A., Ghiassi, M., Kecskeméthy, A. and Papadopoulos, E. "On the effect of semielliptical foot shape on the energetic efficiency of passive bipedal gait," *IEEE/RSJ International Conference on Intelligent Robots and Systems (IROS '19)*, Macau, China, 2019.

[18] Mahmoodi, P., Ransing, R. S., and Friswell, M. I., "Modelling the effect of 'heel to toe' roll-over contact on the walking dynamics of passive biped robots," *Applied Mathematical Modelling*, 2013, 37(12-13): pp. 7352-7373.

[19] Hansen, A. H., Childress, D. S., and Knox, E. H., "Roll-over shapes of human locomotor systems: effects of walking speed," *Clinical biomechanics*, 2004, 19(4): pp. 407-414.

[20] Wei, S. E., Ramakrishna, V., Kanade, T., and Sheikh, Y., "Convolutional pose machines," *IEEE Conference on Computer Vision and Pattern Recognition (CVPR '16)*, Las Vegas, USA, 2016, pp. 4724-4732.

[21] Cao, Z., Simon, T., Wei, S. E., and Sheikh, Y., "Realtime multi-person 2d pose estimation using part affinity fields," *IEEE Conference on Computer Vision and Pattern Recognition (CVPR '17)*, Honolulu, USA, 2017, pp. 7291-7299.

[22] Campbell, S. L., Stephen, L., and Leimkuhler, B., "Differentiation of Constraints in Differential-Algebraic Equations", *Journal of Structural Mechanics*, 1991, 19(1), pp. 19-39.